Inorganic Chemistry

Article

pubs.acs.org/IC

Synthesis and Characterization of Silver(I) Pyrazolylmethylpyridine Complexes and Their Implementation as Metallic Silver Thin Film Precursors

Irene Bassanetti,[†,‡] Christina P. Twist,[§,∥] Myung-Gil Kim,[‡] Afif M. Seyam,[⊥] Hassan S. Bazzi,[⊥] Q. Jane Wang,[§] Yip-Wah Chung,[#] Luciano Marchió,*[,†] Massimiliano Delferro,*[,‡] and Tobin J. Marks*[,‡]

[†]Dipartimento di Chimica, Università degli studi di Parma, Parco Area delle Scienze 17/a, 43100 Parma, Italy

[‡]Department of Chemistry and the Material Research Center, Northwestern University, 2145 Sheridan Road, Evanston, Illinois 60208, United States

[§]Department of Mechanical Engineering, Northwestern University, 2145 Sheridan Road, B224, Evanston, Illinois 60208, United States

[∥]Exponent, Inc., 525 W. Monroe St., Suite 1050, Chicago, Illinois 60661, United States

[⊥]Department of Chemistry, Texas A&M University at Qatar, P.O. Box 23874, Doha, Qatar

[#]Department of Materials Science and Engineering, Northwestern University, 2145 Sheridan Road, Evanston, Illinois 60208, United States

Supporting Information

ABSTRACT: A series of light- and air-stable silver(I) pyrazolylmethylpyridine complexes $[Ag(L^R)]_n(BF_4)_n$ (L = pyrazolylmethylpyridine; R = H, **1**; R = Me, **2**; R = i-Pr, **3**) and $[Ag(L^R)(NO_3)]_2$ (L = pyrazolylmethylpyridine; R = H, **4**; R = Me, **5**; R = i-Pr, **6**) has been synthesized and structurally and spectroscopically characterized. In all of the molecular structures, the pyrazolylmethylpyridine ligands bridge two metal centers, thus giving rise to dinuclear (**2**, **4**, **5**, and **6**) or polynuclear structures (**1** and **3**). The role played by the counteranions is also of relevance, because dimeric structures are invariably obtained with NO_3^- (**4**, **5**, and **6**), whereas the less-coordinating BF_4^- counteranion affords polymeric structures (**1** and **3**). Also, through atoms-in-molecules (AIM) analysis of the electron density, an argentophilic Ag···Ag interaction is found in complexes **2** and **4**. Thermogravimetric analysis (TGA) shows that the thermolytic properties of the present complexes can be significantly modified by altering the ligand structure and counteranion. These complexes were further investigated as thin silver film precursors by spin-coating solutions, followed by annealing at 310 °C on 52100 steel substrates. The resulting polycrystalline cubic-phase Ag films of ∼55 nm thickness exhibit low levels of extraneous element contamination by X-ray photoelectron spectroscopy (XPS). Atomic force microscopy (AFM) and scanning electron microscopy (SEM) indicate that film growth proceeds primarily via an island growth (Volmer−Weber) mechanism. Complex **4** was also evaluated as a lubricant additive in ball-on-disk tribological tests. The results of the friction evaluation and wear measurements indicate a significant reduction in wear (∼ 88%) at optimized Ag complex concentrations with little change in friction. The enhanced wear performance is attributed to facile shearing of Ag metal in the contact region, resulting from thermolysis of the silver complexes, and is confirmed by energy-dispersive X-ray analysis of the resulting wear scars.

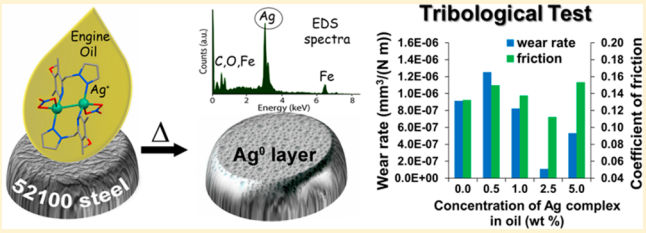

INTRODUCTION

The excellent characteristics of metallic silver coatings, such as a great thermal and oxidative stability, high chemical resistance, high melting point, softness, plasticity, and high electrical conductivity compared to polymeric coatings or other carbonaceous materials, make them excellent candidates for technological applications that include bactericidal coatings,[1] coatings for superconducting materials,[2] optical filters,[3] electrodes for dielectric layers,[4] solid lubricants,[5] and contacts in microelectronic circuitry.[6] Silver films have been deposited by many techniques that can be divided into nonvapor phase (electrodeposition,[7] sol−gel,[8] photochemical deposition[9]) and vapor phase (sputtering,[5w,10] pulsed laser deposition,[11] electron-beam evaporation,[12] chemical vapor deposition[5d,n,6]) techniques. The choice of the deposition technique is strictly related to the chemical and physical properties of the silver precursor and the nature of the substrate. The design of silver precursors is therefore as important as the growth technique in order to achieve superior films for applications. It has also been shown

Received: February 10, 2014
Published: April 18, 2014

   dx.doi.org/10.1021/ic500321w | Inorg. Chem. 2014, 53, 4629−4638

that precursor counterions can play a key role, such as in supramolecular architectures where they can influence the ultimate physicochemical properties.[13] In principle, coordinating counterions can also complete the coordination sphere of the metal ion and tune precursor reactivity for specific technology properties (i.e., facilitating film formation by controlling the thermal stability of the precursor).[14]

Silver complexes have garnered much attention as additives for tribological applications, because the organic ligand stabilizes the high oxidation state of silver, promoting a lower decomposition temperature. In addition, the decomposition temperature can be tuned by modifying the ligand structure, tailored for the particular additive application. The function of the organic ligand is to deliver and release (decomposition) metallic silver to the point of contact. Silver−organic complexes are chosen as additives in this study instead of pure silver metal nanoparticles or inorganic silver salts for multiple reasons, such as ease of synthesis, environmental stability, and relatively low decomposition temperatures. Metallic silver nanoparticles are more difficult to synthesize and require a stabilizing suspension, or surfactant, to avoid nanoparticle aggregation, whereas $AgNO_3$ decomposes at 440 °C, which is well above the typical operating temperature of engine oils. The intended applications of these silver−organic complex additives are for use in heavy duty vehicles or machinery that operate at extremely high temperatures and may experience liquid lubricant starvation, at which point the use of a solid lubricant to supplement base oil would assist in a more stable operation of the lubricated engine components.

One of the primary issues in metallic silver deposition is the final film purity, in that ligand decomposition can leave residual organic contaminants such as P, B, N, and halogens. The requirements for the design of optimal metal−organic silver precursors include: (i) straightforward, cheap, high-yield ligand synthesis; (ii) tunable precursor decomposition temperature so that the onset of metallic film growth can be customized for the application; (iii) both light and air stability so that the precursor is easily stored and handled. A significant number of silver precursors have been reported for various growth processes, ranging from β-diketonates to carboxylates, lactams and olefins, isocyanides, thioureas, and tertiary phosphine adducts.[15] A principal goal in recent years has been the realization of silver precursors which achieve metallic film growth at relatively low temperatures.

In the present investigation, we report the synthesis and characterization of new air- and light-stable silver precursors for thin film growth. The goal is to obtain high-purity silver films with minimal contaminants. The present precursor complexes contain pyrazolylmethylpyridine *N*,*N*′ donor ligands, the hydrophobicity and steric properties of which are modulated by the substituents on the pyrazole 3 and 5 positions (Scheme 1). The molecular structures of these precursor complexes are elucidated by single-crystal X-ray diffraction. In most cases, the compounds have dinuclear structures with ligand-supported argentophilic interactions. To evaluate counteranion influence on physicochemical properties with particular focus on efficacy of silver film growth, two types of counteranions are employed: non/weakly coordinating BF_4^- and coordinating NO_3^-. Furthermore, substituting NO_3^- for BF_4^- should avoid fluoride contaminants during thermally activated film growth while lowering thermolysis temperatures if redox properties are involved. Here, the growth of thin silver films on 52100 steel surfaces is performed via a solution-phase technique. The resulting film properties are characterized by scanning electron microscopy (SEM) and atomic force microscopy (AFM), with characterization of film composition by energy dispersive X-ray spectroscopy (EDS), X-ray photoelectron spectrometry (XPS), and glancing X-ray diffraction (GXRD). It will be shown here that metallic silver films can be grown with negligible traces of contaminants (silver oxide and carbon). Furthermore, the complex $[Ag(L^H)(NO_3)]_2$ (**4**, see below) is evaluated as an engine oil lubricant additive using a standard ball-on-disk tribological test and is shown to be promising for wear reduction.[16]

Scheme 1. Molecular Structures of the Pyrazolylmethylpyridine Ligands L^H, L^{Me}, and L^{iPr}

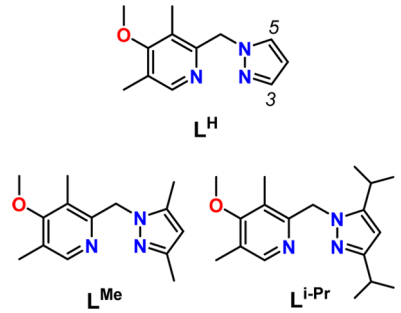

EXPERIMENTAL SECTION

Materials and Methods. All reagents and solvents were purchased from Sigma-Aldrich and used as received. All deuterated solvents (99+ atom %D) were purchased from Cambridge Isotope Laboratories and used as received. The ligand syntheses were performed as previously reported.[17] The 52100 steel bar stock was cut into 1 cm × 1 cm squares and polished to ∼10 nm roughness as measured by AFM. Elemental analyses were performed by Midwest Microlabs, Inc. Indianapolis, Indiana (U.S.A.) and Galbraith Laboratory, Knoxville, Tennessee (U.S.A.). NMR spectra were recorded on a Bruker Avance 300 spectrometer (FT; 300 MHz, ^{1}H) and Bruker AVANCEIII spectrometer (FT; 125 MHz, ^{13}C). Chemical shifts (δ) for ^{1}H and ^{13}C spectra were referenced using internal solvent resonances and are reported relative to tetramethylsilane (TMS). FTIR spectra (4000−700 cm^{-1}) were recorded on a Nicolet Nexus spectrophotometer equipped with a Smart Orbit HATR diamond crystal accessory. An LTQ XL linear ion trap instrument (Thermo Electron Corporation) equipped with an ESI/API Ion Max source was used for mass spectrometry. The ESI source was connected to a solvent delivery system (Finnigan Surveyor, MS Pump Plus) that was used to pump a continuous flow of methanol solution (200 μL min^{-1}). Instrumental tuning was performed by direct infusion of freshly prepared methanol solution (1 nM) of **1**−**6** into the continuous flow of methanol from the pump. Working parameters were set as follows: spray voltage, 3.5 kV; capillary voltage, 15 V; capillary temperature, 200 °C; tube lens, 65 V. Samples were analyzed in flow injection mode using a six-port valve equipped with a 2 μL sample loop. Mass spectra were recorded in full scan analysis mode in the range 0−1500 m/z. Thermogravimetric analysis (TGA) was performed on a TA Q50 ultramicro balance instrument (ramp rate = 5 °C min^{-1} and under a N_2 flow rate of 90 mL min^{-1} at atmospheric pressure. The silver precursor solution (0.08 M in THF/DMSO 4:1 v/v) was spin-coated onto 52100 steel substrates at a speed of 1000 rpm with an acceleration of 1500 rpm/sec for 2 min. The spin-coated films were then annealed on a hot plate at 310 °C for 10 min. Film thicknesses were measured with a Veeco Dektak 150 surface profilometer, and film chemical compositions were assessed with an Omicron ESCA Al Kα probe X-ray photoelectron spectrometer (XPS) under high vacuum (<10^{-8} Torr). Ag film phase purity was also examined using θ−2θ scans on a computer-interfaced Rigaku DMAX-A powder diffrac-

dx.doi.org/10.1021/ic500321w | Inorg. Chem. 2014, 53, 4629−4638

tometer using Ni-filtered Cu Kα radiation. Glancing angle/incidence X-ray diffraction (GXRD; angle of incidence α = 0.3°) θ–2θ scans were recorded on a computer-interfaced Rigaku ATX-G diffractometer. Film microstructure and morphologies were assessed with a Hitachi S4800–II scanning electron microscope (SEM) and a Digital Instruments Nanoscope III atomic force microscope (AFM) operating in the contact mode.

Synthesis of Silver Complexes 1–6. *$[Ag(L^H)]_n(BF_4)_n$ (1).* A solution of $AgBF_4$ (77 mg, 0.39 mmol) in 5 mL of acetone was added to a solution of $\mathbf{L^H}$ (100 mg, 0.39 mmol) in 5 mL of acetone. After 15 min of stirring, the solvent was concentrated under vacuum, and a white solid was precipitated after addition of diethyl ether. The solid was collected by filtration and dried to yield $[Ag(L^H)]_n(BF_4)_n$ (**1**) as a white microcrystalline powder (117 mg, 65%). Colorless crystals suitable for X-ray data collection were obtained by layering diethyl ether over an acetone solution of **1**. IR (cm^{-1}): 3118w, 2942w, 1594w, 1479m, 1446w, 1403m, 1293m, 1271 m, 1238w, 1014s, 882m, 767s, 641m, 608m, 520m. ^{1}H NMR (300 MHz, acetone-d_6): δ = 2.34 (s, 3H, CH_3), 2.51 (s, 3H, CH_3), 3.91 (s, 3H, CH_3O), 5.89 (s, 2H, CH_2), 6.56 (t, J = 2.1 Hz, 1H, CH pyrazole), 7.79 (d, J = 2.1 Hz, 1H, CH pyrazole), 8.26 (d, J = 1.4 Hz, 1H, CH pyrazole), 8.42 (s, 1H, CH pyridine) ppm. ^{13}C NMR (125 MHz, $CDCl_3$): δ = 11.73, 24.5, 58.01, 60.96, 107.62, 129.38, 134.26, 143.23, 152.38, 153.58 ppm. Anal. Calcd for $C_{12}H_{15}AgBF_4N_3O$ (411.94): C, 34.99; H, 3.67; N, 10.20. Found: C, 35.24; H, 3.64; N, 9.87%. ESI-MS (p.i., CH_3OH, m/z, I%): 324.02, $[Ag(L)]^+$; 541.15, $[Ag(L)_2]^+$.

$[Ag(L^{Me})]_2(BF_4)_2$ (2). The procedure used to prepare **1** was applied to a mixture of $AgBF_4$ (73 mg, 0.37 mmol) in 5 mL of acetone and $\mathbf{L^{Me}}$ (105 mg, 0.37 mmol) in 5 mL of acetone. A white microcrystalline powder of $[Ag(L^{Me})]_2(BF_4)_2$ (**2**) was obtained (112 mg, 65%). Colorless crystals suitable for X-ray data collection were obtained by layering hexane over a CH_2Cl_2 solution of **2** corresponding to $[Ag(L^{Me})]_2(BF_4)_2{\cdot}CH_2Cl_2$. IR ($cm^{-1}$): 2970w, 2926w, 2860w, 1594w, 1556m, 1485m, 1403m, 1293m, 1254m, 1019s, 986s, 887w, 805m, 520m.^{1}H NMR (300 MHz, acetone-d_6): δ = 2.24 (s, 3H, CH_3), 2.31 (s, 3H, CH_3), 2.51 (s, 6H, 2 CH_3), 3.91 (s, 3H, OCH_3), 5.64 (s, 2H, CH_2), 6.16 (s, 1H, CH pyrazole), 8.33 (s, 1H, CH pyridine) ppm. ^{13}C NMR (125 MHz, $CDCl_3$): δ 11.54, 11.68, 13.67, 14.48, 54.27, 60.94, 107.43, 128.70, 128.98, 143.88, 150.88, 152.35, 153.75, 167.18 ppm. Anal. Calcd for $C_{28}H_{38}Ag_2B_2F_8N_6O_2$ (880.00): C, 38.22; H, 4.35; N, 9.55. Found: C, 37.07; H, 4.28; N, 9.61%. ESI-MS (p.i., CH_3OH, m/z, I%): 246.16, $[LH]^+$; 352.05, $[Ag(L)]^+$; 597.21, $[Ag(L)_2]^+$.

$[Ag(L^{i\text{-}Pr})]_n(BF_4)_n$ (3). The procedure used to prepare **1** was applied to a mixture of $AgBF_4$ (65 mg, 0.33 mmol) in 5 mL of acetone and $\mathbf{L^{i\text{-}Pr}}$ (100 mg, 0.33 mmol) in 5 mL of acetone. A pale pink microcrystalline powder of $[Ag(L^{i\text{-}Pr})]_n(BF_4)_n$ (**3**) was obtained (131 mg, 79%). Colorless crystals suitable for X-ray data collection were obtained by layering diethyl ether over a methanolic solution of **3**. IR (cm^{-1}): 2964w, 2931w, 2866w, 1578w, 1540w, 1468m, 1402w, 1282m, 1260m, 1172w, 1041s, 991s, 882w, 789m, 515m. ^{1}H NMR (300 MHz, acetone-d_6): δ 1.26 (d, J = 4.6 Hz, 6H, CH_3 i-Pr), 1.31 (d, J = 4.6 Hz, 6H, CH_3 i-Pr), 2.30 (s, 3H, CH_3 pyridine), 2.54 (s, 3H, CH_3 pyridine), 2.99 (m, 1H, CH i-Pr), 3.36 (m, 1H, CH i-Pr), 3.90 (s, 3H, OCH_3), 5.63 (s, 2H, CH_2), 6.29 (s, 1H, CH pyrazole), 8.27 (s, 1H, CH pyridine) ppm. ^{13}C NMR (125 MHz, $CDCl_3$): δ = 11.57, 13.60, 23.10, 23.34, 29.41, 52.91, 60.85, 100.13, 128.11, 128.68, 151.96, 152.55, 153.84, 161.06, 166.92 ppm. Anal. Calcd for $C_{18}H_{27}AgBF_4N_3O$ (496.11): C, 43.58; H, 5.49; N, 8.48. Found: C, 43.18; H, 5.42; N, 8.30%. ESI-MS (p.i., CH_3OH, m/z,I%): 302.22, $[LH]^+$; 408.12, $[Ag(L)]^+$; 597.21, $[Ag(L)_2]^+$.

$[Ag(L^H)(NO_3)]_2$ (4). A solution of $AgNO_3$ (145 mg, 0.86 mmol) in 2 mL of water was added to a solution of $\mathbf{L^H}$ (216 mg, 0.86 mmol) in 5 mL of methanol. The mixture was stirred for 15 min. The solvent was then removed under vacuum, and hexane (5 mL) was added. After 5 min of ultrasonic titration, a white solid precipitated and was collected by filtration and dried to yield $[Ag(L^H)(NO_3)]_2$ (**4**) as white microcrystalline powder (271 mg, 75%). Colorless crystals suitable for X-ray data collection were obtained by layering hexane over a CH_2Cl_2 solution of **4**. ^{1}H NMR (500 MHz, acetone-d_6): δ = 2.29 (s, 3H, CH_3), 2.52 (s, 3H, CH_3), 3.86 (s, 3H, OCH_3), 5.75 (s, 2H, CH_2), 6.47 (t, J = 2.1 Hz, 1H, CH pyrazole), 7.71 (d, J = 2.1 Hz, 1H, CH pyrazole), 8.14 (d, J = 2.4 Hz, 1H, CH pyrazole), 8.34 (s, 1H, CH pyridine) ppm. ^{13}C NMR (125 MHz, acetone-d_6): δ = 11.58, 13.35, 55.63, 61.07, 107.59, 127.75, 128.45, 132.64, 142.28, 151.88, 153.56, 166.34 ppm. Anal. Calcd for $C_{24}H_{30}Ag_2N_8O_8$ (774.29): C, 37.23; H, 3.91; N, 14.47. Found: C, 37.29; H, 3.93; N, 14.37. ESI-MS (p.i., CH_3OH, m/z, I%): 106.91, $[Ag]^+$; 150.09, $[PyCH]^+$; 218.13, $[LH]^+$; 324.03, $[Ag(L)]^+$; 388.18, $[Ag(L)(NO_3)H]^+$; 541.15, $[Ag(L)_2]^+$.

$[Ag(L^{Me})(NO_3)]_2$ (5). The same procedure used to prepare **4** was applied to a mixture of $AgNO_3$ (129 mg, 0.76 mmol) in 2 mL of water and $\mathbf{L^{Me}}$ (214 mg, 0.76 mmol) in 5 mL of methanol. A white solid was precipitated using diethyl ether, which was filtered and dried to yield $[Ag(L^{Me})(NO_3)]_2$ (**5**) (182 mg, 53%). Colorless crystals suitable for X-ray data collection were obtained by layering hexane over a CH_2Cl_2 solution of **5** corresponding to $[Ag(L^{Me})(NO_3)]_2{\cdot}1/2(H_2O){\cdot}1/2(CH_2Cl_2)$. ^{1}H NMR (300 MHz, acetone-d_6): δ = 2.17 (s, 3H, CH_3), 2.23 (s, 3H, CH_3), 2.45 (s, 3H, CH_3), 2.46 (s, 3H, CH_3), 3.84 (s, 3H, OCH_3), 5.51 (s, 2H, CH_2), 6.04 (s, 1H, CH pyrazole), 8.16 (s, 1H, CH pyridine) ppm. ^{13}C NMR (125 MHz, acetone-d_6): δ = 11.61, 11.62, 13.58, 14.29, 52.20, 60.56, 106.57, 127.01, 127.98, 142.51, 149.41, 151.16, 154.36, 166.10 ppm. Anal. Calcd for $C_{28}H_{38}Ag_2N_8O_8$ (830.50):C, 40.50; H, 4.61; N, 13.49. Found: C, 40.73; H, 4.63; N, 13.77. ESI-MS (p.i., CH_3OH, m/z, I%): 106.91, $[Ag]^+$; 150.09, $[PyCH]^+$; 246.16, $[LH]^+$; 352.06, $[Ag(L)]^+$; 599.21, $[Ag(L)_2]^+$.

$[Ag(L^{i\text{-}Pr})(NO_3)]_2$ (6). Complex **6** was synthesized using the same procedure employed to prepare **4** but with a mixture of $AgNO_3$ (117 mg, 0.69 mmol) in 2 mL of water and $\mathbf{L^{i\text{-}Pr}}$ (207 mg, 0.69 mmol) in 5 mL of methanol. A white solid was precipitated with diethyl ether which was collected by filtration and dried to yield $[Ag(L^{i\text{-}Pr})(NO_3)]_2$ (**6**) (130 mg, 40%). Colorless crystals suitable for X-ray data collection were obtained by layering hexane over a THF solution of **6**. ^{1}H NMR (300 MHz, acetone-d_6): δ = 1.25 (d, J = 4.8 Hz, 6H, CH_3 i-Pr), 1.27 (d, J = 4.5 Hz, 6H, CH_3 i-Pr), 2.29 (s, 3H, CH_3), 2.50 (s, 3H, CH_3), 3.00 (m, 1H, CH i-Pr), 3.29 (m, 1H, CH i-Pr), 3.83 (s, 3H, OCH_3), 5.58 (s, 2H, CH_2), 6.21 (s, 1H, CH pyrazole), 8.30 (s, 1H, CH pyridine) ppm. ^{13}C NMR (125 MHz, acetone-d_6): δ 11.60, 14.29, 23.16, 26.61, 51.48, 60.34, 99.91, 127.24, 128.20, 151.93, 151.93, 152.83, 160.50, 172.94 ppm. Anal. Calcd for $C_{36}H_{54}Ag_2N_8O_8$ (942.61): C, 45.87; H, 5.77; N, 11.89. Found: C, 45.74; H, 5.82; N, 11.79. ESI-MS (p.i., CH_3OH, m/z, I%): 106.90, $[Ag]^+$; 302.22, $[LH]^+$; 408.12, $[Ag(L)]^+$; 711.34, $[Ag(L)_2]^+$.

Single Crystal X-ray Structures. Single-crystal data were collected with a Bruker Smart APEXII area detector diffractometer (Mo Kα; λ = 0.71073 Å). Cell parameters were refined from the observed setting angles and detector positions of selected strong reflections (Table S1). Intensities were integrated from several series of exposure frames that covered the sphere of reciprocal space.[18] A multiscan absorption correction was applied to the data using the program SADABS.[19] The structures were solved by direct methods[20] and refined with full-matrix least-squares (SHELXL-97),[21] using the Wingx software package.[22] Graphical material was prepared with the Mercury 3.0 program.[23]

Tribology Experiments. The lubricating quality of oil–silver complex mixtures was evaluated through ball-on-disk tests using a UMT high-temperature tribotester.[5a,16] Silver complex **4** was combined with 15W-40 military-grade engine oil with a viscosity of 0.26 Pa·s at 25 °C. The complex was dissolved in a minimal amount of DMSO[24] (1.3 mL per 1 g silver complex) and then added to the oil to achieve complex concentrations of 0.5, 1.0, 2.5, and 5.0 wt %. Before testing, the oil–silver complex mixtures were stirred vigorously with a magnetic stir bar for at least 30 min to ensure homogeneous dispersion of the silver complexes in the base oil. This mixture was applied to the disk surface immediately prior to ball-on-disk friction tests to provide flooded lubrication at the point of contact. The balls were made of M50 bearing steel with 62 HRC hardness and a diameter of 4 mm. Disks were 51200 steel typically used in bearings, heat-treated to 50 HRC hardness, then ground and polished to a mirror finish. Tests applied a 25 N vertical load to the stationary ball, which contacted the disk rotating at 200 rpm. Real-time friction measurements were recorded over the duration of the tests. After friction tests were

dx.doi.org/10.1021/ic500321w | Inorg. Chem. 2014, 53, 4629–4638

completed, disks were cleaned in an acetone ultrasonic bath. Measurements of the wear scar were made using an ADE phase Shift MicroXAM white light interferometer. Each additive concentration in oil was tested twice for friction and wear performance. Heating coils surrounding the disk maintained a chamber temperature of 200 °C throughout the 30 min tests. This temperature was chosen to replicate the higher end of operating temperatures in an internal combustion engine.[25]

RESULTS AND DISCUSSION

Silver Precursor Synthesis and Characterization. The synthesis of the new pyrazolylmethylpyridine silver(I) complexes with two different counteranions (NO_3^- and BF_4^-) is first presented. The solid-state molecular structures are then discussed, and on the basis of thermogravimetric data, three of these compounds are selected for metallic silver thin film growth on 52100 steel substrates. These thin silver layers are then fully characterized by means of AFM, XPS, GXRD, and SEM techniques in order to analyze the morphology and purity of the metallic films.

The ligand syntheses were previously described[17] and are briefly summarized in Scheme 2. A phase-transfer catalyst ($Bu_4N^+OH^-$) is employed due to the differing solubilities of pyrazole (water) and chloromethylpyridine (toluene). The steric encumbrance of the pyrazoles influences the reactivity and ultimately the final yield, although the ligands are obtained in moderate to good yields. These ligands were previously investigated in regard to their coordination behavior with Zn^{2+} and Cu^{2+} with which they yielded mononuclear or dinuclear complexes, with the ligand always behaving as an *N,N′* bidentate chelate.[17] In the present contribution, we wished to investigate their behavior with respect to a softer metal ion such as Ag^+, for which low coordination number complexes are common. The synthesis of the present silver complexes is performed at room temperature using equimolar amounts of ligands and $AgBF_4$ or $AgNO_3$ (Scheme 3). The presence of the nitrate anion gives rise to dinuclear complexes, whereas with BF_4^-, dinuclear complexes and two polymeric structures are obtained instead (vide infra). The complexes were fully characterized in solution by means of NMR techniques and ESI-MS spectrometry. Specifically, ESI-MS spectrometry provides useful information on molecular aggregation, which in turn can influence thermolysis pathways. In fact, Ag^+ and $[Ag(L)_2]^+$ signals are identified in the ESI mass spectra of all complexes (Supporting Information, Figures S1−S6), even at very low cone voltage. The occurrence of such species suggests the lability of the dinuclear/polynuclear complexes, the fragmentation of which may represent the initial step in silver film deposition. X-ray crystallographic results reveal that complexes $[Ag(L^H)]_n(BF_4)_n$ (**1**) and $[Ag(L^{i\text{-}Pr})]_n(BF_4)_n$ (**3**), reported in Figure 1 and Table 1, exhibit similar polymeric structures. In both structures, the Ag^+ ion exhibits a distorted linear geometry, with a N(21)−Ag−N(13) angle of 159.59(2)° for **1** and 168.2(2)° for **3**. In both structures, the $Ag-N_{pyrazole}$ coordination distance (2.145(3) and 2.132(5) Å) is significantly shorter than that $Ag-N_{pyridine}$ coordination distance (2.176(3)

Scheme 2. Synthesis of Pyrazolylmethylpyridine Ligands L^H, L^{Me}, and L^{iPr}

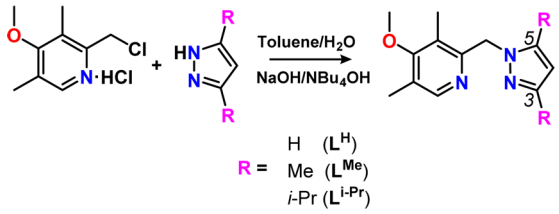

Scheme 3. Synthesis of Silver Complexes 1−6

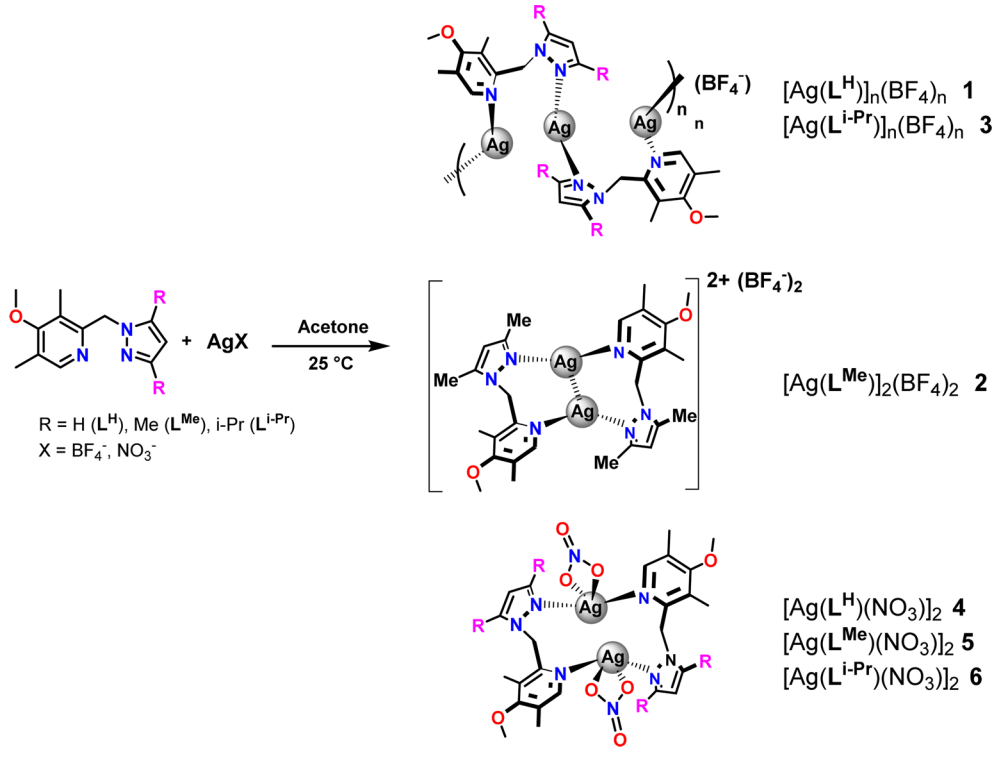

dx.doi.org/10.1021/ic500321w | Inorg. Chem. 2014, 53, 4629−4638

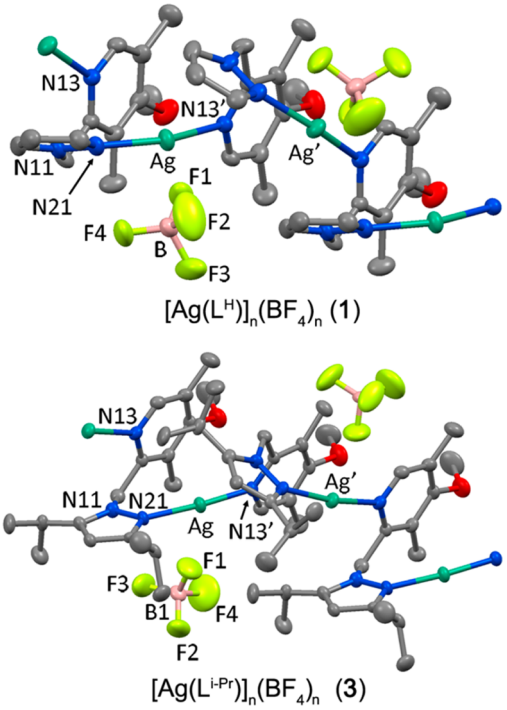

Figure 1. Molecular structures of complexes **1** (above, ′ = $x + 1/2, 1/2 - y, z$) and **3** (below, ′ = $x, 1 - y, 1/2 + z$). Thermal ellipsoids are drawn at the 30% probability level. Hydrogen atoms are omitted for clarity.

Table 1. Relevant Bond Distances (Å) and Angles (deg) for Complexes $[Ag(L^H)]_n(BF_4)_n$, $[Ag(L^{Me})]_2(BF_4)_2{\cdot}CH_2Cl_2$, and $[Ag(L^{i\text{-}Pr})]_n(BF_4)_n$[a]

$[Ag(L^H)]_n(BF_4)_n$			
Ag–N(21)	2.145(3)	N(21)–Ag–N(13)′	159.6(1)
Ag–N(13)′	2.176(3)	N(21)–Ag–F(1)	79.4(2)
Ag–F(1)	2.829(5)	F(1)–Ag–N(13)′	120.5(2)
$[Ag(L^{Me})]_2(BF_4)_2{\cdot}CH_2Cl_2$			
Ag(1)–N(24)	2.112(3)	N(24)–Ag(1)–N(13)	166.8(1)
Ag(1)–N(13)	2.147(3)	N(21)–Ag(2)–N(16)	167.7(1)
Ag(2)–N(21)	2.115(3)	Ag(2)–Ag(1)–N(13)	65.44(8)
Ag(2)–N(16)	2.141(3)	N(24)–Ag(1)–Ag(2)	101.44(8)
Ag(1)–Ag(2)	3.309(1)	N(21)–Ag(2)–Ag(1)	101.42(8)
		N(16)–Ag(2)–Ag(1)	66.36(7)
$[Ag(L^{i\text{-}Pr})]_n(BF_4)_n$			
Ag–N(21)	2.132(5)	N(21)–Ag–N(13)[#]	168.6(2)
Ag–N(13)[#]	2.153(6)	N(21)–Ag–F(1)	82.4(4)
Ag–F(1)	2.794(5)	F(1)–Ag–N(13)[#]	93.0(4)

[a]Please note that the symbol in parentheses (′) = $x + 1/2, 1/2 - y, z$. Please note that the symbol in parentheses (#) = $x, 1 - y, 1/2 + z$.

and 2.153(6) Å) (Table 1). A weak interaction between the BF_4^- counteranion is responsible for the metal geometry distortion (d[Ag···F(1)] = 2.829(5) Å for **1** and 2.794(5) Å for **3**).[26] The nitrogen atoms of the pyrazole and pyridine rings point in nearly opposite directions and are bound to different silver ions. This generates a coordination polymer molecular chain that can be viewed as a zigzag chain. In contrast, the complex $[Ag(L^{Me})]_2(BF_4)_2$ (**2**) reported in Figure 2 exhibits a dinuclear structure in which two metal ions are bound by two *N,N′* donor ligands. The Ag^+ ion is in a distorted linear geometry with N–Ag–N coordination angles of ∼167°. The distortion from the ideal linear geometry is presumably a

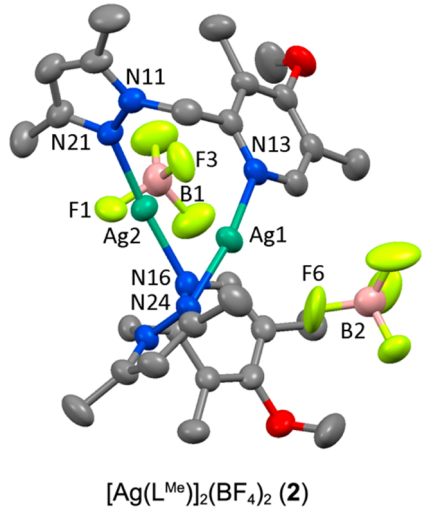

Figure 2. Molecular structure of complex **2**. Thermal ellipsoids are drawn at the 30% probability level. Hydrogen atoms are omitted for clarity.

consequence of the Ag···F interaction between the metal ion and the disordered BF_4^- anion (Ag···F distance ≈2.7 Å). In this complex, the two metal ions give rise to a weak Ag···Ag argentophilic interaction, as evidenced by the intermetallic distance of 3.309(1) Å, which is slightly less than the v.d.W. radii sum (3.44 Å).[27] Note that using the more strongly coordinating NO_3^- anion in place of BF_4^-, dinuclear structures are invariably observed. In fact, the complexes $[Ag(L^H)(NO_3)]_2$ (**4**), $[Ag(L^{Me})(NO_3)]_2$ (**5**), and $[Ag(L^{i\text{-}Pr})(NO_3)]_2$ (**6**) have very similar molecular structures (Figures 3 and 4; Table 2) in which two silver ions are bridged by two *N,N′* donor ligands, and the coordination is completed by nitrate anions.

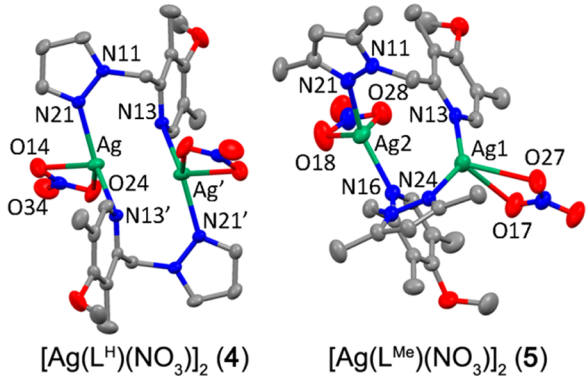

Figure 3. Molecular structures of complexes **4** (left) and **5** (right). Thermal ellipsoids are drawn at the 30% probability level. Hydrogen atoms are omitted for clarity.

In all of the present structures, the Ag^+ ions assume coordination geometries that are intermediate between trigonal planar and the distorted tetrahedral. In fact, the NO_3^- anions act as O,O bidentate ligands but are coordinated unsymmetrically to the metal centers, with one of the Ag···O distances invariably longer than the other, as summarized in Table 2.[28] The structure of complex **5** differs slightly from that of **4** in that it exhibits a different mutual orientation of the two ligands in the dinuclear entity (Figure 3). The asymmetric unit of complex **6** (Figure 4) is composed of two distinct molecular

dx.doi.org/10.1021/ic500321w | Inorg. Chem. 2014, 53, 4629–4638

Table 2. Relevant Bond Distances (Å) and Angles (deg) for Complexes $[Ag(L^{H})(NO_3)]_2$, $[Ag(L^{Me})(NO_3)]_2 \cdot 1/2(H_2O) \cdot 1/2(CH_2Cl_2)$, and $[Ag(L^{i\text{-}Pr})(NO_3)]_2$[a]

$[Ag(L^{H})(NO_3)]_2$			
Ag–N(21)	2.237(3)	N(21)–Ag–N(13)′	131.8(1)
Ag–O(14)	2.627(3)	N(21)–Ag–O(24)	121.3(1)
Ag–O(24)	2.508(4)	N(13)′–Ag–O(24)	106.9(1)
Ag–N(13)′	2.309(3)	N(21)–Ag–O(14)	89.0(1)
Ag–Ag′	2.945(1)	N(13)′–Ag–O(14)	126.0(1)
$[Ag(L^{Me})(NO_3)]_2 \cdot 1/2(H_2O) \cdot 1/2(CH_2Cl_2)$			
Ag(1)–N(24)	2.184(5)	N(24)–Ag(1)–N(13)	141.9(2)
Ag(1)–N(13)	2.227(5)	N(24)–Ag(1)–O(17)	112.8(2)
Ag(1)–O(17)	2.590(6)	N(24)–Ag(1)–O(27)	104.8(2)
Ag(1)–O(27)	2.629(5)	N(13)–Ag(1)–O(27)	113.1(2)
Ag(2)–N(21)	2.168(5)	N(13)–Ag(1)–O(17)	96.6(2)
Ag(2)–N(16)	2.219(5)	N(21)–Ag(2)–N(16)	147.5(2)
Ag(2)–O(18)	2.540(5)	N(21)–Ag(2)–O(18)	110.3(2)
Ag(2)–O(28)	2.639(7)	N(21)–Ag(2)–O(28)	107.1(2)
Ag(1)–Ag(2)	4.163(1)	N(16)–Ag(2)–O(18)	102.1(2)
		N(16)–Ag(2)–O(28)	96.2(2)
$[Ag(L^{i\text{-}Pr})(NO_3)]_2$			
Ag(1)–N(21)	2.170(6)	N(21)–Ag(1)–N(16)	126.9(2)
Ag(1)–N(16)	2.284(6)	N(21)–Ag(1)–O(213)	137.3(2)
Ag(1)–O(213)	2.431(6)	N(16)–Ag(1)–O(213)	94.2(2)
Ag(1)–O(113)	2.569(6)	N(16)–Ag(1)–O(113)	109.2(2)
Ag(2)–N(24)	2.201(6)	N(21)–Ag(1)–O(113)	114.3(2)
Ag(2)–N(13)	2.267(6)	N(24)–Ag(2)–N(13)	129.9(2)
Ag(2)–O(114)	2.472(7)	N(24)–Ag(2)–O(114)	115.7(2)
Ag(2)–O(214)	2.672(6)	N(13)–Ag(2)–O(114)	114.5(2)
Ag(3)–N(27)	2.265(6)	N(24)–Ag(2)–O(214)	117.5(2)
Ag(3)–N(112)	2.279(6)	N(13)–Ag(2)–O(214)	97.4(2)
Ag(3)–O(115)	2.461(7)	N(27)–Ag(3)–N(112)	122.4(2)
Ag(3)–O(215)	2.512(7)	N(27)–Ag(3)–O(115)	134.1(2)
Ag(4)–N(210)	2.196(5)	N(112)–Ag(3)–O(115)	98.6(3)
Ag(4)–N(19)	2.245(6)	N(27)–Ag(3)–O(215)	114.2(2)
Ag(4)–O(116)	2.550(7)	N(112)–Ag(3)–O(215)	118.5(3)
Ag(4)–O(116)	2.585(7)	N(210)–Ag(4)–N(19)	137.5(2)
Ag(1)–Ag(2)	4.373(2)	N(210)–Ag(4)–O(116)	108.1(2)
Ag(3)–Ag(4)	4.584(2)	N(19)–Ag(4)–O(116)	109.7(2)
		N(210)–Ag(4)–O(116)	118.1(2)
		N(19)–Ag(4)–O(116)	95.4(2)

[a]Please note that the symbol in parentheses (′) = 1 − *x*; −*y*; −*z*.

fragments (Figure 4A,B) as a consequence of the different bridging geometries of the NO_3^- anion. The O(116) oxygen atom bound to Ag(4) links together two dinuclear entities, thus forming a tetranuclear complex, whereas the O(114) atom in the first dinuclear entity interacts only weakly with the Ag(2) ion of an adjacent dimer (Ag(2)–O(114)′ = 2.863(9) Å, ′ = 1 − *x*; −*y*; −*z*). In complex **6**, the pyridine rings of each dinuclear moiety give rise to a partial *π*-stack (N(13)–N(16) = 3.29(1) Å, C(53)–C(56) = 3.35(1) Å for one dimer, and N(19)–N(112) = 3.29(1) Å, C(59)–C(512) = 3.27(1) Å) for the second dimer. Interestingly, in **4**, the short Ag···Ag distance of 2.945(1) Å supports the presence of a weak Ag···Ag interaction. This type of interaction is absent in **5** and **6**, judging by the Ag···Ag distances within the dimers, which exceed 4 Å.[27e] The atoms-in-molecules (AIM) analysis of electron density[29] has proven to be a powerful tool for studying various chemical interactions.[30] AIM analysis was applied to dinuclear complexes **2**, **4**, and **5** in order to substantiate the assertion that a metal–metal interaction is present in **2** and **4** as judged by the short

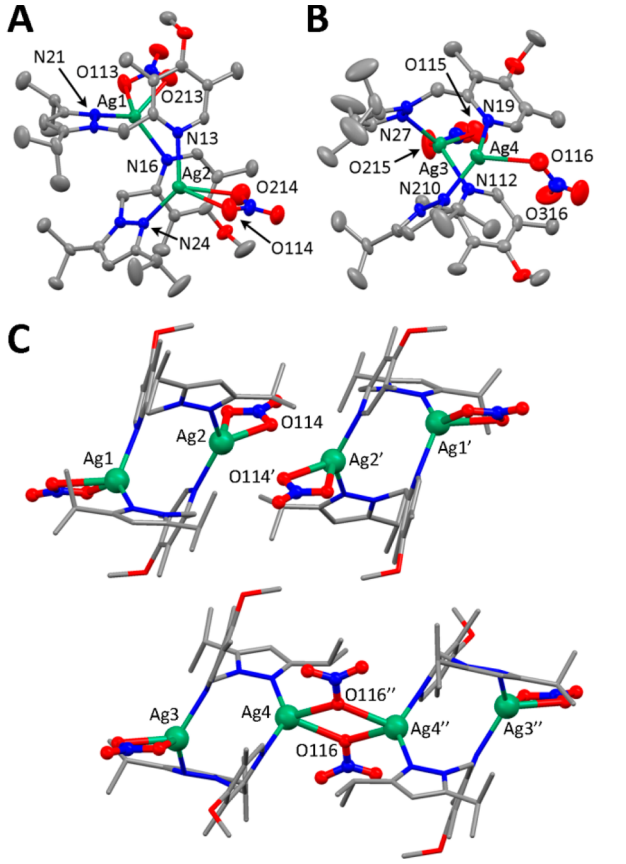

Figure 4. (A and B) Molecular structures of the two dinuclear entities that comprise the asymmetric unit of **6** with hydrogen atoms omitted for clarity. Solid thermal ellipsoids are reported at the 30% probability level. (C) Portion of the crystal packing of **6** showing the different environments of the two dinuclear entities. Symmetry codes: ′ = 1 − *x*; −*y*; −*z*. ″ = 1 − *x*; −*y*; 1 − *z*.

intermetallic distances. Because **5** and **6** exhibit very similar geometries, the AIM analysis was applied only for **5** as representative of both structures. This analysis shows that there is a significant electron density accumulation between the two Ag centers in **2** and **4**, as confirmed by the presence of a bond critical point (BCP). In contrast, there is no BCP in the intermetallic region of **5**, in agreement with the longer intermetallic distance (see the Supporting Information (SI), Figures S12–S14).

In all of the molecular structures reported, the pyrazolylmethylpyridine ligands bridge two Ag centers, affording polynuclear (**1** and **3**) or dinuclear (**2**, **4**, **5**, and **6**) structures. Despite the different molecular arrangements, both types of structures can be described as in Scheme 4. The presence of the central methylenic spacers between the pyridine and pyrazole rings imparts substantial conformational flexibility to the ligands, but in none of the present structures do the ligands adopt a conformation that is suitable for chelating a single metal center.[31] The role played by the anions is also relevant, because dimeric structures are invariably obtained with NO_3^- (**4**, **5**, and **6**), whereas the less-coordinating BF_4^- anion preferentially yields polymeric structures (**1** and **3**). It can be tentatively proposed that the greater coordinative capabilities of NO_3^-, when compared to BF_4^-, saturate the stereoelectronic requirements of Ag^+, leading to the formation of complexes with lower nuclearity. For the sake of completeness, note that

dx.doi.org/10.1021/ic500321w | Inorg. Chem. 2014, 53, 4629–4638

Scheme 4. Schematic Description of the Ligand Arrangements in the Present Dinuclear and Polynuclear Pyrazolylmethylpyridine Complexes

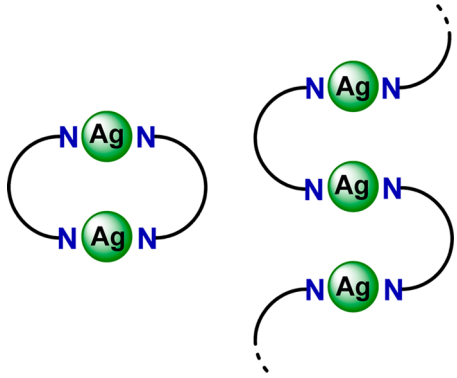

several complexes have been reported with pyrazolylmethylpyridine ligands in which the pyridine ring is unsubstituted.[32] In particular, pyrazolylmethylpyridine ligands were extensively used for the complexation of transition metal ions in mononuclear complexes,[33] whereas dinuclear complexes with nickel, palladium, and cobalt have been reported in which the anions acts as bridging units between two metal−ligand moieties.[34]

Silver Complex Thermolysis. Atmospheric pressure thermogravimetric analysis (TGA) of silver complexes **1**−**6** was performed under N_2 to evaluate the temperature at which they undergo thermolysis. Powder X-ray diffraction (PXRD) and X-ray photoelectron spectroscopy (XPS) were then performed to gain insight into the composition of the residual material. TGA and PXRD data for **1**−**6** are reported in Figure 5. By inspection of the TGA profiles, it is evident that the complexes containing the NO_3^- anion (**4**−**6**) have increased weight loss at lower temperatures than the BF_4^- complexes (**1**−**3**). The PXRD analysis of the thermolysis products confirms the presence of metallic silver. For all complexes, the residual weight corresponds to the calculated weight percentage for silver with an additional weight percentage (∼10%) due to the

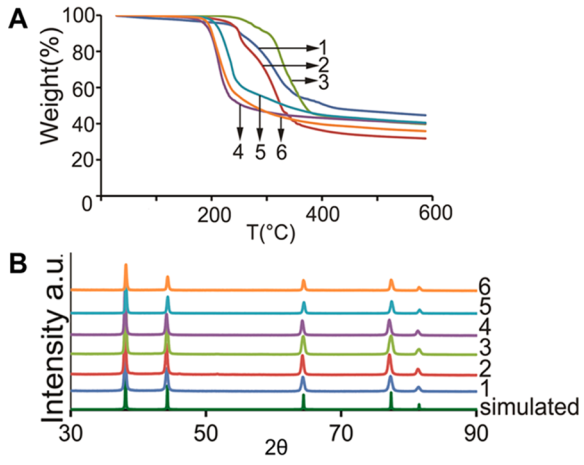

Figure 5. (A) Atmospheric pressure thermogravimetric analysis (TGA) of complexes **1**−**6**. The weight loss data were recorded at the ramp rate of 5 °C min^{-1} and a 90 mL min^{-1} N_2 flow rate. (B) X-ray powder diffractograms performed on residues of **1**−**6** after the thermolysis. The simulated spectrum of cubic phase metallic silver is shown for comparison (PDF 04-0783).

formation of amorphous carbonaceous material (confirmed by elemental analysis: C, 9.27; H, 0.12%) and a very thin Ag_2O layer on the surface.[35] From the molecular structures discussed above, the presence of the coordinating NO_3^- anion affords neutral molecular assemblies whereas the weakly interacting BF_4^- anion leads to complexes with greater ionic character. Furthermore, NO_3^- is a stronger oxidizing agent which may assist ligand decomposition.[14] Thus, silver film deposition on 52100 steel substrates was investigated with complexes **4**−**6**.

Silver Film Deposition and Surface Analysis. As indicated in the previous section, complexes **4**−**6** were investigated for metallic silver film deposition on 52100 steel substrates according to their promising thermolysis properties. Silver thin film formation on clean 52100 steel coupons was investigated under varied deposition conditions, including silver complex concentration (0.02 to 0.1 M), solvent (acetone, THF, methanol, *t*-butanol, DMSO), temperature (180−400 °C), time (2, 5, 10, 20 min), and spin-coating rate (200 to 2000 rpm). Overall, optimum thin film performance (homogeneity, roughness, and thickness) is achieved with spin-coating at 1000 rpm of 0.08 M solutions of complexes **4**−**6** in 4:1 THF/DMSO followed by annealing at 310 °C for 10 min. This procedure yields Ag films with an average thickness of ∼55 nm and an AFM-derived RMS roughness of ∼18.5 nm. The morphology of the Ag thin films was analyzed by SEM (Figure 6A) and AFM (Figure 6B). The AFM image of the **4**-derived film shows a relatively homogeneous deposition on the substrate, implying an island growth mechanism (Volmer−Weber) typical of Ag film growth on oxide and semiconductor surfaces.[36] Some accumulation of the metal in certain areas is probably due to the rapid heating. The results obtained for **5** and **6** are comparable to those of **4**, and these are reported in the SI (Figures S19−S20). In addition, energy-dispersive X-ray spectroscopic analysis (EDS, Figure 6C) confirms a preponderance of Ag on the 52100 steel substrate. The purity of the Ag film was also investigated by X-ray photoelectron spectroscopy (XPS) and glancing angle/incidence X-ray diffraction (GXRD; Figure 7). The XPS spectra exhibit characteristic metallic Ag $3d_{5/2}$ and $3d_{3/2}$ signatures,[37] with negligible traces of contaminants, whereas the GXRD reveals cubic metallic Ag. Due to the limited film thickness/inhomogeneity of the thin films, both XPS and GXRD exhibit additional peaks typical of the 52100 steel substrate (XPS: Fe, O, and C, Figure S21)[38] and Ag_2O. The latter contaminant arises from surface oxidation of the Ag film.

Evaluation of Silver Complex 4 as a Lubricant Additive. Friction and Wear Measurements. High temperature ball-on-disk tests were performed to evaluate complex **4** as a lubricant additive at 200 °C.[16] Formulated 15W-40 engine oil containing various concentrations of complex **4** (0.5, 1, 2.5, and 5.0 wt %, with a minimum amount of DMSO) provided fully flooded lubrication between the steel ball and disk. Figure 8A shows the average friction measured over the 30 min tests, in addition to wear measurements of the resulting wear scars on the disks. The wear rate is the volume of material removed from the surface of the disk per unit sliding distance, normalized by the applied load. No appreciable difference in the coefficient of friction is noted between the four oil−silver complex mixtures. However, higher concentrations (2.5 and 5 wt %) of the silver complex in oil result in significantly reduced wear compared to the pure oil, with a remarkable 88% reduction in average wear rate at 2.5 wt %. In addition, EDS analysis reveals small amounts of silver-based particles[39] in the

dx.doi.org/10.1021/ic500321w | Inorg. Chem. 2014, 53, 4629−4638

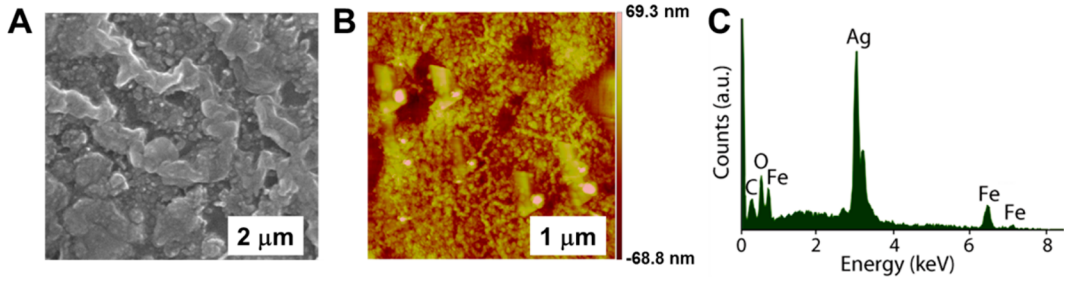

Figure 6. Images of the thin Ag film deposited on a 52100 steel substrate after thermolysis of compound **4**. (A) Scanning electron microscopy (SEM). (B) Atomic force microscopy (AFM) image, R_{rms} = 18.5 nm. (C) Energy-dispersive X-ray spectroscopy (EDS) spectrum of the Ag layer.

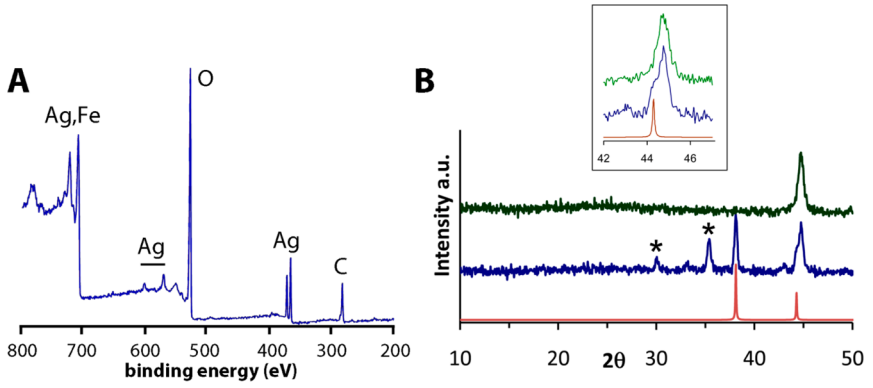

Figure 7. Ag film deposited on 52100 steel substrate after thermolysis of **4**. (A) XPS spectrum. (B) GXRD diffractogram (θ–2θ) in blue. Peak positions and relative intensities for the powder pattern of cubic phase Ag (PDF 04-0783) are presented in red. The GXRD diffractogram of the 52100 steel is given in green for comparison. * = Ag_2O.

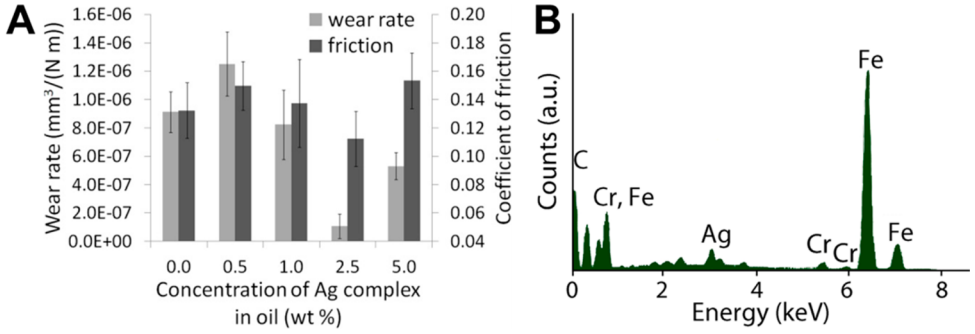

Figure 8. (A) Measured wear rate and coefficient of friction for ball-on-disk tests using various amounts of silver complex **4** in oil. Error bars represent ± one standard deviation. (B) EDS spectrum of a sample area in a wear scar after tribological testing.

wear scar, along with other elements (mainly, Fe and Cr) composing the 52100 steel disk (Figure 8B). These findings provide evidence to the protective effect exhibited by compound **4** when employed as an antiwear additive in oil.

■ CONCLUSIONS

Six cationic silver complexes with pyrazolylmethylpyridine ligands and BF_4^- (**1**–**3**) and NO_3^- (**4**–**6**) counteranions were synthesized and chemically/structurally characterized. The complexes with NO_3^- exhibit dinuclear structures with the NO_3^- strongly coordinated to the metal center. In contrast, the BF_4^--containing complexes have more varied molecular geometries, including dinuclear and polynuclear structures. In all cases, BF_4^- is only weakly coordinated to Ag^+, implying a more pronounced ionic character in **1**–**3** than in **4**–**6**. This is also reflected in the TGA profiles, with complexes **4**–**6** being less thermally stable. Given the low decomposition temperatures, **4**–**6** were further investigated as silver film precursors using spin-coated films, followed by annealing at 310 °C. The resulting 55 nm films are composed primarily of metallic silver with traces of Ag_2O and carbon impurities (assessed by EDS, XPS, and GXRD). Moreover, preliminary tribological studies show that complex **4**, $[Ag(L^H)(NO_3)]_2$, when added to engine oil at 2.5 and 5 wt %, provides significant wear reduction. The enhanced wear performance is attributed to the lubricious properties of pure metal silver, which is a thermolytic product of the complex at elevated temperatures. Deposition of the silver-based complexes in the wear scar is confirmed by energy-dispersive X-ray analysis.

■ ASSOCIATED CONTENT

Supporting Information

ESI-MS spectra of complexes **1**–**6**, X-ray powder diffraction of complexes **2**–**6**. Atoms-in-molecules (AIM) analysis of the

dx.doi.org/10.1021/ic500321w | Inorg. Chem. 2014, 53, 4629–4638

electron density. Silver layer characterization: glancing X-ray diffraction, atomic force microscopy, scanning electron microscopy, and energy dispersive X-ray spectroscopy. This material is available free of charge via the Internet at http://pubs.acs.org. CCDC 818740−818742 and 906519−906521 contain the supplementary crystallographic data for this paper. These data can be obtained free of charge from The Cambridge Crystallographic Data Centre via www.ccdc.cam.ac.uk/data_request/cif.

AUTHOR INFORMATION

Corresponding Authors

*E-mail: (L.M.) luciano.marchio@unipr.it.
*E-mail: (M.D.) m-delferro@northwestern.edu.
*E-mail: (T.J.M) t-marks@northwestern.edu.

Notes

The authors declare no competing financial interest.

ACKNOWLEDGMENTS

This publication was made possible by National Priorities Research Program (NPRP grant no. 5-192-1-046) from the Qatar National Research Fund (a member of the Qatar Foundation) and the U.S. Army Tank-Automotive and Armaments Command (TACOM contract no. W56HZV-09-0341). The statements made herein are solely the responsibility of the author(s). Purchases of the NMR and GC-TOF instrumentation at IMSERC were supported by the National Science Foundation (CHE-1048773 and CHE-0923236, respectively). Microscopy studies made use of the EPIC facility (NUANCE Center-Northwestern University), which has received support from the MRSEC program (NSF DMR-1121262) at the Materials Research Center, and the Nanoscale Science and Engineering Center (EEC-0118025/003), both programs of the National Science Foundation, the State of Illinois, and Northwestern University. Financial support from the University of Parma is also acknowledged. I.B. thanks the University of Parma (Italy) for a study leave. The authors also thank Polyera Corp. for assistance with the profilometric analysis.

REFERENCES

(1) Yuan, Z.; Dryden, N. H.; Li, X.; Vittal, J. J.; Puddephatt, R. J. *J. Mater. Chem.* **1995**, *5*, 303−308.

(2) (a) Iida, K.; Kono, T.; Kaneko, T.; Katagiri, K.; Sakai, N.; Murakami, M.; Koshizuka, N. *Supercond. Sci. Technol.* **2004**, *17*, S46−S50. (b) Harnois, C.; Desgardin, G.; Laffez, I.; Chaud, X.; Bourgault, D. *Physica C* **2002**, *383*, 269−278. (c) Kalyanaraman, R.; Oktyabrsky, S.; Narayan, J. *J. Appl. Phys.* **1999**, *85*, 6636−6641. (d) Lee, D.; Chaud, X.; Salama, K. *Jpn. J. Appl. Phys.* **1992**, *31*, 2411−2419.

(3) Piszczek, P.; Szlyk, E.; Chaberski, M.; Taeschner, C.; Leonhardt, a.; Bala, W.; Bartkiewicz, K. *Chem. Vapor Depos.* **2005**, *11*, 53−59.

(4) (a) Prudenziati, M.; Morten, B.; Gualtieri, A. F.; Leoni, M. *J. Mater. Sci.: Mater. Electron.* **2004**, *15*, 447−453. (b) Dellacorte, C.; Pepper, S. V.; Honecy, F. S. *Surf. Coat. Technol.* **1992**, *52*, 31−37.

(5) (a) Twist, C. P.; Seyam, A. M.; Chen, C.; Kim, M.-G.; Weberski, M. P.; Ren, N.; Marks, T. J.; Chung, Y.-W.; Wang, Q. J. *Adv. Eng. Mater.* **2012**, *14*, 101−105. (b) Mulligan, C. P.; Blanchet, T. A.; Gall, D. *Surf. Coat. Technol.* **2010**, *204*, 1388−1394. (c) Baraket, M.; Mercs, D.; Zhang, Z. G.; Coddet, C. *Surf. Coat. Technol.* **2010**, *204*, 2386−2391. (d) Guo, Y.; Wang, D.; Liu, S. *Appl. Surf. Sci.* **2010**, *256*, 1714−1719. (e) Mulligan, C. P.; Blanchet, T. A.; Gall, D. *Wear* **2010**, *269*, 125−131. (f) Zhang, H.-S.; Endrino, J. L.; Anders, A. *Appl. Surf. Sci.* **2008**, *255*, 2551−2556. (g) Mulligan, C. P.; Blanchet, T. A.; Gall, D. *Surf. Coat. Technol.* **2008**, *203*, 584−587. (h) Zheng, X. H.; Tu, J. P.; Lai, D. M.; Peng, S. M.; Gu, B.; Hu, S. B. *Thin Solid Films* **2008**, *516*, 5404−5408. (i) Weng, L. J.; Sun, J. Y.; Hu, M.; Gao, X. M.; Xue, Q. J. *Vacuum* **2007**, *81*, 997−1002. (j) Basnyat, P.; Luster, B.; Kertzman, Z.; Stadler, S.; Kohli, P.; Aouadi, S.; Xu, J.; Mishra, S. R.; Eryilmaz, O. L.; Erdemir, A. *Surf. Coat. Technol.* **2007**, *202*, 1011−1016. (k) Aouadi, S. M.; Paudel, Y.; Luster, B.; Stadler, S.; Kohli, P.; Muratore, C.; Hager, C.; Voevodin, A. A. *Tribol. Lett.* **2007**, *29*, 95−103. (l) Wang, Q.; Tu, J. P.; Zhang, S. C.; Lai, D. M.; Peng, S. M.; Gu, B. *Surf. Coat. Technol.* **2006**, *201*, 1666−1670. (m) Li, B.; Wang, X.; Liu, W.; Xue, Q. *Tribol. Lett.* **2006**, *22*, 79−84. (n) Yao, S. H.; Su, Y. L.; Kao, W. H.; Cheng, K. W. *Surf. Coat. Technol.* **2006**, *201*, 2520−2526. (o) Lungu, C. P. *Surf. Coat. Technol.* **2005**, *200*, 198−202. (p) Lungu, C. P.; Mustata, I.; Musa, G.; Zaroschi, V.; Mihaela Lungu, A.; Iwasaki, K. *Vacuum* **2004**, *76*, 127−130. (q) Wang, W. *Surf. Coat. Technol.* **2004**, *177−178*, 12−17. (r) Mosaner, P.; Bonelli, M.; Miotello, A. *Surf. Coat. Technol.* **2004**, *180−81*, 41−43. (s) Gomez-Vega, J. M.; Teshima, K.; Hozumi, A.; Sugimura, H.; Takai, O. *Surf. Coat. Technol.* **2003**, *169−170*, 504−507. (t) Endrino, J. L.; Nainaparampil, J. J.; Krzanowski, J. E. *Surf. Coat. Technol.* **2002**, *157*, 95−101. (u) Sliney, H. E.; Loomis, W. R.; DellaCorte, C. *Surf. Coat. Technol.* **1995**, *76−77*, 407−414. (v) Maréchal, N.; Pauleau, Y.; Quesnel, E.; Juliet, P.; Rouzaud, A.; Zimmermann, C. *Surf. Coat. Technol.* **1994**, *68−69*, 416−421. (w) Maréchal, N.; Quesnel, E.; Pauleau, Y. *Thin Solid Films* **1994**, *241*, 34−38. (x) Spalvins, T.; Sliney, H. E. *Surf. Coat. Technol.* **1994**, *68−69*, 482−488.

(6) (a) Gao, L.; Härter, P.; Linsmeier, C.; Wiltner, A.; EmLing, R.; Schmitt-Landsiedel, D. *Microelectron. Eng.* **2005**, *82*, 296−300. (b) Manepalli, R.; Stepniak, F.; Bidstrup-Allen, S. A.; Kohl, P. A. *IEEE Trans. Adv. Packag.* **1999**, *22*, 4−8.

(7) Xu, X. H.; Hussey, C. L. *J. Electrochem. Soc.* **1992**, *139*, 1295−1300.

(8) (a) Zhao, Y.; Yang, B.; Xu, J.; Fu, Z.; Wu, M.; Li, F. *J. Sol−Gel Sci. Technol.* **2012**, *61*, 577−584. (c) Ivanova, T.; Harizanova, A.; Koutzarova, T.; Vertruyen, B. *Cryst. Res. Technol.* **2012**, *47*, 579−584.

(9) Yonezawa, Y.; Sato, T.; Kuroda, S.; Kuge, K.-I. *J. Chem. Soc., Faraday Trans.* **1991**, *87*, 1905.

(10) (a) Chiu, K.-F.; Blamire, M. G.; Barber, Z. H. *J. Vac. Sci. Technol., A* **1999**, *17*, 2891−2895. (b) Yang, F.-L.; Somekh, R. E.; Greer, A. L. *Thin Solid Films* **1998**, *322*, 46−55.

(11) (a) De, B. A.; Galasso, A.; Ibris, N.; Sansone, M.; Santagata, A.; Teghil, R. *Surf. Coat. Technol.* **2012**, *207*, 279−285. (b) Alonso, J. C.; Diamant, R.; Castillo, P.; Acosta-Garcia, M. C.; Batina, N.; Haro-Poniatowski, E. *Appl. Surf. Sci.* **2009**, *255*, 4933−4937. (c) Kumar, P.; Krishna, M. G.; Bhatnagar, A. K.; Bhattacharya, A. K. *J. Mater. Res.* **2008**, *23*, 1826−1839. (d) Donnelly, T.; Doggett, B.; Lunney, J. G. *Appl. Surf. Sci.* **2006**, *252*, 4445−4448.

(12) Nakanishi, Y.; Miyake, A.; Kominami, H.; Aoki, T.; Hatanaka, Y.; Shimaoka, G. *Appl. Surf. Sci.* **1999**, *142*, 233−236.

(13) (a) Bassanetti, I.; Mezzadri, F.; Comotti, A.; Sozzani, P.; Gennari, M.; Calestani, G.; Marchiò, L. *J. Am. Chem. Soc.* **2012**, *134*, 9142−9145. (b) Halper, S. R.; Do, L.; Stork, J. R.; Cohen, S. M. *J. Am. Chem. Soc.* **2006**, *128*, 15255−15268. (c) Campos-Fernández, C. S.; Schottel, B. L.; Chifotides, H. T.; Bera, J. K.; Bacsa, J.; Koomen, J. M.; Russell, D. H.; Dunbar, K. R. *J. Am. Chem. Soc.* **2005**, *127*, 12909−12923.

(14) (a) Kim, M.-G.; Hennek, J. W.; Kim, H. S.; Kanatzidis, M. G.; Facchetti, A.; Marks, T. J. *J. Am. Chem. Soc.* **2012**, *134*, 11583−11593. (b) Hennek, J. W.; Kim, M.-G.; Kanatzidis, M. G.; Facchetti, A.; Marks, T. J. *J. Am. Chem. Soc.* **2012**, *134*, 9593−9596. (c) Kim, M.-G.; Kanatzidis, M. G.; Facchetti, A.; Marks, T. J. *Nat. Mater.* **2011**, *10*, 382−388.

(15) (a) Panneerselvam, A.; Nguyen, C. Q.; Malik, M. a.; O'Brien, P.; Raftery, J. *J. Mater. Chem.* **2009**, *19*, 419. (b) McCain, M. N.; Schneider, S.; Salata, M. R.; Marks, T. J. *Inorg. Chem.* **2008**, *47*, 2534−2542. (c) Grodzicki, A.; Łakomska, I.; Piszczek, P.; Szymańska, I.; Szłyk, E. *Coord. Chem. Rev.* **2005**, *249*, 2232−2258. (d) Edwards, D. A.; Harker, R. M.; Mahon, M. F.; Molloy, K. C. *J. Mater. Chem.* **1999**, *9*, 1771−1780.

(16) Twist, C. P.; Bassanetti, I.; Snow, M.; Delferro, M.; Bazzi, H.; Chung, Y. W.; Marchió, L.; Marks, T. J.; Wang, Q. J. *Tribol. Lett.* **2013**, *52*, 261−269.
(17) (a) Tardito, S.; Bassanetti, I.; Bignardi, C.; Elviri, L.; Tegoni, M.; Mucchino, C.; Bussolati, O.; Franchi-Gazzola, R.; Marchiò, L. *J. Am. Chem. Soc.* **2011**, *133*, 6235−6242. (b) Gennari, M.; Tegoni, M.; Lanfranchi, M.; Pellinghelli, M. A.; Marchio, L. *Inorg. Chem.* **2007**, *46*, 3367−3377.
(18) *SMART Version 5.054 Data Collection and SAINT-Plus Version 6.02A: Data Processing Software for the SMART System*; Bruker Analytical X-Ray Instruments, Inc.: Madison, WI, 2000.
(19) *Area-Detector Absorption Correction*; Siemens Industrial Automation, Inc.: Madison, WI, 1996.
(20) Burla, M. C.; Caliandro, R.; Camalli, M.; Carrozzini, B.; Cascarano, G. L.; De Caro, L.; Giacovazzo, C.; Polidori, G.; Spagna, R. *J. Appl. Crystallogr.* **2005**, *38*, 381−388.
(21) Sheldrick, G. M. *SHELX97*; Programs for Crystal Structure Analysis, 1997.
(22) Farrugia, L. J. *J. Appl. Crystallogr.* **1999**, *32*, 837−838.
(23) Macrae, C. F.; Edgington, P. R.; McCabe, P.; Pidcock, E.; Shields, G. P.; Taylor, R.; Towler, M.; van de Streek, J. *J. Appl. Crystallogr.* **2006**, *39*, 453−457.
(24) The EPA has classified DMSO as "practically non toxic". For example, see Vignes, R. P. Abstract of Papers, 220th ACS National meeting, Washington, DC, United states, August 20−24, 2000, IEC-091.
(25) Priest, M.; Taylor, C. M. *Wear* **2000**, *241*, 193−203.
(26) The average distances found in the Cambridge Crystallographic Data centre (CDC, Oct. 2012) for Ag···F−BF_3 (weak) interaction = 2.598 Å.
(27) (a) Sculfort, S.; Braunstein, P. *Chem. Soc. Rev.* **2011**, *40*, 2741−2760. (b) Katz, M. J.; Sakai, K.; Leznoff, D. B. *Chem. Soc. Rev.* **2008**, *37*, 1884−1895. (c) Doerrer, L. H. *Comment Inorg. Chem.* **2008**, *29*, 93−127. (d) Che, C.-M.; Lai, S.-W. *Coord. Chem. Rev.* **2005**, *249*, 1296−1309. (e) Pyykkö, P. *Chem. Rev.* **1997**, *97*, 597−636.
(28) In regard to the issue of whether the above single crystal results are representative of the bulk material, powder X-ray diffraction (PXRD) data of bulk microcrystalline **1**, **3**, **4**, and **6** correspond well to randomly oriented power patterns generated from the single crystal X-ray analysis (Figures S7−S11). Note, however, that the PXRD patterns of **2** and **5** are not superimposable on the simulated pattern derived from the single-crystal X-ray analyses (Figures S8, S10). This may reflect the presence of cocrystallization solvents in the unit cells of the **2** and **5** single crystals (see the Experimental Section), which are not present in the microcrystalline materials used for the powder diffraction.
(29) (a) Bader, R. F. W. *J. Phys. Chem. A* **1998**, *102*, 7314−7323. (b) Bader, R. F. W. *Chem. Rev.* **1991**, *91*, 893−928. (c) Bader, R. F. W. *Atoms in Molecules: A Quantum Theory*; Oxford University Press: New York, 1994.
(30) (a) Serpe, A.; Artizzu, F.; Marchiò, L.; Mercuri, M. L.; Pilia, L.; Deplano, P. *Cryst. Growth Des.* **2011**, *11*, 1278−1286. (b) García, M. E.; Ramos, A.; Ruiz, M. A.; Lanfranchi, M.; Marchio, L. *Organometallics* **2007**, *26*, 6197−6212. (c) Molina Molina, J.; Dobado, J. A.; Heard, G. L.; Bader, R. F. W. *Theor. Chim. Acta* **2001**, *105*, 365−373. (d) Llusar, R.; Beltrán, A.; Andrés, J.; Fuster, F.; Silvi, B. *J. Phys. Chem. A* **2001**, *105*, 9460−9466.
(31) Bassanetti, I.; Marchio, L. *Inorg. Chem.* **2011**, *50*, 10786−10797.
(32) Mukherjee, R. *Coord. Chem. Rev.* **2000**, *203*, 151−218.
(33) (a) Ojwach, S. O.; Nyamato, G. S.; Omondi, B.; Darkwa, J. *Inorg. Chim. Acta* **2012**, *392*, 141−147. (b) Segapelo, T. V.; Guzei, I. A.; Spencer, L. C.; Van Zyl, W. E.; Darkwa, J. *Inorg. Chim. Acta* **2009**, *362*, 3314−3324. (c) Balamurugan, V.; Hundal, M. S.; Mukherjee, R. *Chem.—Eur. J.* **2004**, *10*, 1683−1690.
(34) (a) Ojwach, S. O.; Guzei, I. A.; Benade, L. L.; Mapolie, S. F.; Darkwa, J. *Organometallics* **2009**, *28*, 2127−2133. (b) Bai, S.-Q.; Gao, E.-Q.; He, Z.; Fang, C.-J.; Yan, C.-H. *New J. Chem.* **2005**, *29*, 935−941.
(35) (a) Kariniemi, M.; Niinistö, J.; Hatanpää, T.; Kemell, M.; Sajavaara, T.; Ritala, M.; Leskelä, M. *Chem. Mater.* **2011**, *23*, 2901−2907. (b) Yang, C.; Xie, Y. T.; Yuen, M. M. F.; Xu, B.; Gao, B.; Xiong, X. M.; Wong, C. P. *Adv. Funct. Mater.* **2010**, *20*, 2580−2587. (c) Lyu, L. M.; Wang, W. C.; Huang, M. H. *Chem.—Eur. J.* **2010**, *16*, 14167−14174.
(36) (a) Samoilenkov, S.; Stefan, M.; Wahl, G.; Paramonov, S.; Kuzmina, N.; Kaul, A. *Chem. Vapor Depos.* **2002**, *8*, 74−78. (b) Venables, J. A.; Derrien, J.; Janssen, A. P. *Surf. Sci.* **1980**, *95*, 411−430.
(37) *Handbook of X-ray Photoelectron Spectroscopy*; Chastain, J., King, R. C., Eds.; Physical Electronics: Eden Prairie, MN, 1995.
(38) Hirsch, M. R.; Neu, R. W. *Tribol. Int.* **2013**, *68*, 77−84.
(39) Due to the limited amount of thermolysis material in the wear scar after the high-temperature ball-on-disk test, the nature of the Ag-based particles was not investigated by X-ray photoelectron spectroscopy (XPS) and glancing incidence X-ray diffraction GXRD.